Prediction of contact characteristics of abrasive belt compliant grinding for aircraft blades

Jihao Duan (flydjh@163.com)
Xi'an University of Technology
Zhuofan Wu
Jiale An
Dou Wang
Feng Gao
Wenbo Huai

Research Article

Keywords: Aircraft blade, compliance wheel, belt grinding, pressure distribution, contact characteristics

Posted Date: June 1st, 2023

DOI: https://doi.org/10.21203/rs.3.rs-2995012/v1

Abstract

Due to the characteristics of thin-walled curved surface, wall thickness variations and processing cantilever fixtures, the mechanical state of the different contact positions of aircraft engine blades varies significantly during the grinding process. The different contact interactions between contact wheel and blade result in changes of material removal efficiency and surface quality. To achieve contact state control during blade grinding process, a novel flexible abrasive belt grinding device was designed and developed considering the compliance of rubber contact wheel. The significant effect of compliance parameters on grinding contact state was verified through simulation. The grinding contact pressure distribution and normal contact force at different positions in the blade width and length directions were studied, and a prediction model for the maximum contact pressure and normal contact force was established based on BP neural networks. The results showed that with the increase in contact wheel compliance, the effective contact range increased, the pressure distribution gradually became uniform, and showed a double-elliptical distribution. The maximum contact pressure was significantly reduced, with a reduction of up to 46.00%. As the grinding contact position moved towards the weak rigidity area of the blade, the contact pressure distribution became more uniform. And the normal contact force was significantly reduced, with a maximum reduction of 68.49%. The mean average percentage error (MAPE) of the prediction model was small, verifying the effectiveness of the model. The research results of this manuscript laid a foundation for achieving consistent control of blade grinding material removal rate through contact wheel compliance adjustment.

Specific remarks

1) What is your main contribution to the field?

The main contribution of the manuscript is that a novel belt compliant device is proposed and used in blade grinding process. The influence of grinding wheel compliance and different grinding positions on grinding contact characteristics is studied in detail. And the research will help to develop suitable belt grinding process control methods for blades, and realize the prediction of grinding contact pressure and normal contact force.

2) What is novel? In theory, in experimental techniques, or a combination of both?

The novel lies in a combination of both theory and experimental techniques. The novel grinding device is designed considering the effect of hyperelastic rubber wheel deformation on grinding contact mechanism. And the different contact characteristics at different grinding positions of thin-walled blades are analyzed in order to establish the contact pressure and force model based on the simulation and experiment results.

3) Does your paper have industrial applications? If yes, who are the likely user?

Yes, this study has an extensive industrial application. The paper establish an important theoretical foundation for efficient, precise, and intelligent control of blade grinding processes. The enterprises involving the field of aircraft engine manufacturing, free-form surface workpiece manufacturing, especially the blade manufacturing, are the potential users.

1. Introduction

Blades are one of the major critical components of aircraft engines, whose profile accuracy and surface consistency have a significant impact on the aerodynamic efficiency and fatigue life of the engine [1, 2]. Due to their thin-walled and weakly rigid structure, as well as the complex curvature and difficult-to-machine materials, the high-efficiency and precision machining of aircraft blades is facing great challenges.

Currently, precision milling is one of the main technologies for obtaining blade profiles. However, milling processes cannot guarantee the actual profile accuracy and surface quality due to the characteristics of blade thickness, curvature variation, etc. Therefore, precision grinding is often required to remove residual machining allowances of milling process, ensure the profile dimensional accuracy and improve the surface integrity.

Compared with rigid grinding process, belt grinding is an elastic contact grinding process that uses abrasive grains uniformly planted in an elastic substrate to form a grinding tool. Under the guidance of a hyperelastic rubber contact wheel, abrasive belt contacts the blade surface and makes relative movement to remove material from workpiece. It is an important means for the precision grinding process of weakly rigid curved blades [3–5].

However, due to the weak rigidity of blade and the hyperelastic effect of rubber contact wheel, different regions of blades exhibit complex and variable contact states during abrasive belt grinding. And this makes it difficult to control grinding pressure effectively and affects material removal efficiency and processing quality [6]. Therefore, the current blade manufacturing still mostly adopts the inefficient "processing-inspection" method to ensure processing quality [7].

To address these challenges, scholars have focused on the research of robotic abrasive belt grinding force/position control [8–12], parameter optimization [13–15], compensation control [16, 17], etc. Xu et al. [18, 19] proposed a robotic belt grinding force control method that combines force/position compound control with PI/PD control, and analyzed the precision, stability and reliability of the system. Zhang [20] et al. explored a constant force control algorithm based on the pressure release model and model-based reinforcement learning, which is used in the different stages like impact and processing stages. And the optimal parameters were obtained to improve the machining quality. Combining neural network and genetic algorithm, Mohammad et al. [21] proposed a grinding and polishing optimization method for material removal and surface quality improvement. Chen et al. [22] proposed a polishing end effector for intelligent robots and developed a gravity compensation force controller, with which compensation control of polishing force was achieved to attain preferable surface quality.

In the actual manufacturing process, the influence of hyperelastic effect of rubber contact wheel on contact characteristics has not been fully explained. Additionally, the differences of processing state at different grinding points produce a great impact on the grinding contact and machining quality. Therefore, based on the proposed novel grinding device, the influence of compliant contact wheel on grinding pressure distribution and normal contact force was indicated in this manuscript. And the contact mechanism affected by different grinding characteristics of blade at different grinding positions was revealed. Finally, a prediction model of contact pressure was established. The research will help to develop suitable belt grinding process control methods for blades, and realize the prediction of grinding contact pressure and force. Simultaneously, it establish an important theoretical foundation for efficient, precise, and intelligent control of blade grinding processes.

2. Compliant abrasive belt grinding technique of blade

2.1 Belt grinding characteristics of blade

Aircraft engine blades consist of parts such as concave part, convex part, leading and trailing edges. And the leading and trailing edges are usually designed as high-order theoretical free-form surfaces with very small transition sizes to the concave and convex parts. The minimum thickness of some compressor blades is even less than 0.1 mm. Therefore, different ranges of processing deformation are easily accompanied during blade grinding process. The rubber material contact wheel and the blade workpiece are in flexible contact, which is different from the planar contact problem in rigid processing. Under the grinding trajectory control with different technological parameters, a large elastic contact deformation of contact wheel is produced. Meanwhile, the surface structure characteristics (e.g. curvature radius, normal wall thickness) vary at different machining positions, so that a complex and changeable machining state is presented during grinding process. And differences in material removal effect and processing surface quality are caused ultimately. Additionally, blade grinding is usually carried out by cantilever clamping method, which aggravates the complex changes in belt grinding process.

2.2 grinding device with compliance adjustable contact wheel

In order to adapt to the geometric and rigid state changes, a flexible grinding device with compliance adjustable contact wheel was designed as shown in Fig. 1(a) on the basis of basic grinding theory. The compliance of contact wheel is adjusted depending on the support state of hyperelastic rubber material wheel [23, 24]. Through the adjustment of compliance of contact wheel, the contact state between contact wheel and blade can be adaptive controlled.

The designed grinding device consists of rod, tool handle, bearing seat, flange, ribs, guide part, contact wheel, abrasive belt and so on. The core of this grinding device lies in the special structure inside the rubber contact wheel, as shown in Fig. 1(b). The contact wheel is uniformly arranged with arc-shaped rib hole channels inside. The position change of ribs in the channel plays a different supporting role on the

compliance of contact wheel. The control of contact state during the grinding process is realized additionally. The movement of the ribs in the channels of contact wheel is driven by the servo-driven bearing seat under the constraints of guide part. The servo-driven linear displacement variable λ (mm) is defined as 0 mm when all internal ribs are fully inserted into channels, which is used for characterizing the contact wheel compliance.

3. Compliance analysis of contact wheel

3.1 Constitutive model of rubber contact wheel

The rubber contact wheel is one of the key components for abrasive belt grinding. The belt is guided to realize multi-axis machining of curved components. Different from the mechanical properties of metal materials, rubber material is a typical hyperelastic material which has the properties of large elastic deformation, incompressibility and viscoelasticity. Common hyperelastic constitutive models include Mooney-Rivlin, Neo-Hookean, Ogden, Yeoh, etc., which have different application ranges as shown in Table 1. Since the grinding process described in this article belongs to precision machining, with small contact wheel shear deformation of less than 75%, the commonly used Mooney-Rivlin [25] is selected as the constitutive model of contact wheel.

Table 1
Characteristics and application of different hyperelastic constitutive models

Constitutive model	Characteristics and application
Mooney-Rivlin	suitable for rubber with small and medium deformation, but cannot accurately simulate rubber with carbon black
Yeoh	suitable for the large deformation behavior of rubber with carbon black, but can't accurately describe the situation of small deformation
Ogden	Suitable for large deformation environment, still applicable when the strain reaches 700%
Neo-Hookean	The parameters required by the model are simple, and suitable for tensile environment

Mooney Rivlin model is:

$$W = C_1(I_1 - 3) + C_2(I_2 - 3)$$

where W stands for the strain energy density of rubber material; I_1 and I_2 represent the invariants of deformation tensors; C_1 and C_2 denote the material elastic coefficients related to rubber hardness. Since the elastic effect of rubber material is much greater than the elastic property of abrasive belt substrate, the influence of abrasive belt microscopic state on the contact state is not considered in the subsequent research.

3.2 Contact simulation analysis

To reveal the effectiveness of contact wheel compliance in adjusting the machining process, a simulation contact model between the wheel and the blade is established as shown in Fig. 2. The origin of coordinate system O_1-XYZ is located at the center of the convex surface of blade fixed end, where X represents the direction along the width of the blade, Y represents the direction along the length, and Z represents the direction perpendicular to the blade surface. O_2 is the central point of contact wheel. In the simulation model, the aluminum alloy blade is chosen as the object to be machined. The rib is made of 45 steel material, and the contact wheel is made of rubber material with a hardness of 75Hs/A. Other physical property parameters are detailed in Table 2.

Table 2
Physical parameters of simulation model

	Material	Elastic modulus *E*/GPa	Poisson's ratio *v*
Blade	Aluminum alloy	71	0.33
Ribs	45 steel	200	0.3
Contact wheel	Rubber	/	/

Due to the large deformation of the rubber material wheel during the grinding contact process with aluminum alloy blade workpiece, large deflection is initiated during the simulation. The blade surface in contact pair is set as the target surface, while the outer circular surface of contact wheel is set as the contact surface. High-precision hexahedral elements are adopted for the aluminum alloy blade, and the meshes between contact wheel and rebars are segmented. Tetrahedral SOLID92 elements are used to refine the mesh near the contact surface.

In the contact process simulation, the linear length L of the blade is 80mm, the linear width B_1 is 40 mm, the curvature radius R_1 is 40 mm, the contact wheel radius R_2 is 40mm, and the contact wheel width B_2 is 15 mm. A cantilever single-end fixed constraint is applied to blade. The contact wheel speed r is 2000 r/min. The theoretical cutting depth a_p is 0.1 mm. The projection point of the axial center of the contact wheel in the XOY coordinate system is defined as the contact point (x, y). During grinding penetration, the radial direction of contact wheel is always perpendicular to the blade surface. Three points O_1, A and O_2 are collinear.

3.3 Simulation results

The contact state changes between the contact wheel and the workpiece surface during penetration at the contact point (x = 0 mm, y = 7.5 mm) are simulated and analyzed, respectively, under λ = 0, 1, 2 and 5 mm. And the stress distribution of the contact area is derived as shown in Fig. 3.

The preliminary simulation results demonstrate that the wheel compliance λ has a significant impact on the contact pressure distribution between contact wheel and blade workpiece. And the pressure distribution is approximately elliptical. With the increase of λ, the cavity volume inside the contact wheel channel increases, and the compliance of rubber material is enhanced, which makes the contact area larger. However, the pressure distribution of the contact area tends to be more uniform, and the maximum contact pressure decreases significantly. Accordingly, the pressure distribution gradually changes to a double elliptical peak distribution. When λ = 0 and 1 mm, the contact pressure distribution is unimodal, and the maximum contact pressures are 0.191 MPa and 0.125 MPa, respectively. When λ = 2 and 5 mm, the maximum contact pressures are reduced to 0.110 MPa and 0.103 MPa, respectively. Compared to the case of λ = 0 mm, the maximum contact pressure drops by about 0.080 MPa when λ = 5 mm, with a decrease of 46%. By equivalent conversion of contact pressure distribution, the normal contact force is obtained as shown in Fig. 4. With the increase of wheel compliance λ, the normal contact force decreases from 4.611 N to 3.191 N. It can be clearly seen that wheel compliance parameter has a great influence on maximum contact pressure, pressure distribution and distribution area, which can provide a positive effect for grinding process control compensation.

4. Contact characteristic at different positions of blade

Due to the influence of different factors such as wall thickness and curvature at different positions, the contact state consistency of the thin-walled blade clamped by cantilever is poor during the grinding process. And it is difficult to attain stable grinding quality. As the grinding position changes with the X direction, the contact state is affected by the twisting deformation of blade. As the contact position changes with the Y direction, the contact state is affected by the bending deformation of blade.

To clarify the variation trends of grinding contact state at different blade positions, the contact pressure distributions at blade contact points A_1 (0 mm, 7.5 mm), A_2 (10 mm, 7.5 mm) and A_3 (20 mm, 7.5 mm) are initially investigated under λ = 0 mm as shown in Fig. 5. Meanwhile, the equivalent normal contact force under the cross influence of compliance parameter λ and different X-direction positions is obtained as shown in Fig. 6.

The simulation results show that as the contact position deviates in X direction to approach the leading and trailing edge of blade, the wall thickness gradually decreases and the machining rigidity weakens. The contact pressure distribution gradually changes from a single peak value to a multi-peak value distribution state, and the maximum contact pressure gradually decreases from 0.191 MPa to 0.123 MPa, with a decrease of 35.6%. Nonetheless, the pressure distribution changes more uniform. As is clear from the equivalent normal contact force results in Fig. 6, when the contact position changes in X direction, the normal contact force decreases rapidly. When λ = 0 mm, the normal contact force decreases from 4.611 N to 4.113 N and finally to 1.594 N, with two decreases 10.8% and 61.2%, respectively. When λ = 5 mm, the normal contact force decreases from 3.191 N to 2.999 N and finally to 1.295 N, with two decreases of 6.02% and 56.8%, respectively. At the same position in the X direction and under different compliance parameter, there are also significant differences in normal contact force.

Additionally, the different contact positions in Y direction have a significant impact on the grinding contact state of the cantilever-clamped thin-walled workpiece. According to the above mentioned simulation method, the contact simulation of different grinding contact positions within the 7.5–72.5mm region in Y direction is carried out to obtain the contact pressure distribution state as shown in Fig. 7 and the equivalent normal contact force at different positions as shown in Fig. 8.

As the contact position deviates in Y direction and moves away from the cantilevered end of the workpiece, the support rigidity of blade gradually weakens, and the contact pressure distribution gradually becomes flatter and more uniform. Overall, the contact pressure presents a single peak elliptic area distribution, and the maximum contact pressure gradually decreases. At a contact position y = 72.5 mm away from the cantilever end, the maximum contact pressure decreases to 0.084 MPa. Compared with the maximum contact pressure of 0.191 MPa at point y = 7.5mm, the overall decrease is 56.0%. Figure 8 shows that when λ = 0 mm, the equivalent normal contact force decreases significantly as the grinding contact point is away from the constrained end. At the contact position x = 0 mm, the normal contact force decreases from 4.611N to 1.453N.

In summary, the geometrical and spatial characteristics of blade vary in different grinding contact positions in X and Y directions, which affect the machining rigidity at different grinding positions and cause significant differences in grinding contact state. Meanwhile, the wheel compliance parameter λ plays an important role in the grinding state. Hence, to compensate for the differences in grinding process and quality caused by different grinding positions, the contact wheel compliance parameter can be adjusted, which effectively adapts to the changes of blade machining state and provide a method for obtaining consistent machining accuracy and surface quality.

5. Grinding experiments

To verify the reliability of grinding contact simulation, a grinding contact experiment was carried out using a JD50 3-axis CNC machining center. The workpiece used in the experiment was an aluminum alloy blade with the same size and processing parameters as those in the simulation. The normal contact force during the grinding contact process was acquired in real time using an LH-SZ-02 3-axis force sensor. The grinding experimental setup is shown in Fig. 9.

Initially, the grinding contact experiments were carried out under different contact wheel compliance λ. The grinding contact position (0 mm, 20.5 mm) of the blade was selected, and the normal contact force was detected in real time under the conditions of under λ = 0, 1, 2 and 5 mm. The collected normal contact force data is shown in Fig. 10. And the comparison with the simulation results under identical conditions is shown in Fig. 11.

The experimental measurements were assumed to be true values. The experimental results show that at the grinding contact position (0 mm, 20.5 mm), the simulation data has high reliability under different compliance parameter conditions. The maximum error at λ = 0 mm is -0.25 N, and the maximum and minimum relative errors of simulations are 5.53% and 4.12%, respectively. The mean absolute percentage

error is 4.82%, and the root mean square error is 0.177 N. The contact state during compliant abrasive belt grinding is described accurately through simulation.

Secondly, to verify the influence of blade grinding position on the contact state, six positions A ~ F on blade profile were selected, as shown in Fig. 12.The coordinate values were A (20 mm, 20.5 mm), B (20 mm, 46.5 mm), C (20 mm, 72.5 mm), D (0 mm, 20.5mm), E (0 mm, 46.5 mm) and F (0 mm, 72.5 mm), respectively. The grinding contact experiments were carried out under the condition of λ = 0 mm.

The experimental results are compared with the simulation results as shown in Fig. 13. It is clear that under the conditions of λ = 0 mm, x = 0 mm (contact points D, E, F) and λ = 0 mm, x = 20 mm (contact points A, B, C), the normal contact forces decrease with the increase of the distance from the constraint end. The simulation values are in good agreement with the experimental values. The maximum absolute error is -0.38 N, the maximum relative error is 14.29%, the mean absolute percentage error is 10.16%, and the root mean square error is 0.198 N. This indicates that the simulation data has high reliability and also indicates that different contact positions of the blade have a significant effect on its grinding contact state.

6. BP neural network-based prediction of blade contact characteristics

To grasp the variation trends of contact state during blade grinding and realize the prediction of grinding characteristics for targeted control of machining process, a simulation research was carried out by comprehensively considering the influence of wheel compliance parameter λ and contact positions (x, y). Other parameters involved in the simulation process are the same as those in Section 2.2. The variation of the maximum contact pressure and normal contact force is shown in Fig. 14.

The change of contact position actually affects the normal wall thickness, cantilever distance and curvature direction, etc. of blade in the machining process, resulting in the difference of machining state. With the increase of the contact position in Y direction, away from the blade constraint end, the clamping and support effect of the blade is weakened, and the maximum contact pressure of the grinding contact position is significantly reduced. The normal contact force also decreases to varying degrees. When λ = 0 mm and x = 0 mm, with the increase of y, the maximum contact pressure decrease by 55.96% from 0.190 MPa to 0.084 MPa, and the normal contact force decreases by 68.49% from 4.611 N to 1.453 N.

With the increase of the contact position in the X direction, the grinding point tends to approach the thinner leading and trailing edge of blade, and the processing rigidity of the blade is weak and torsional deformation is enhanced. The maximum contact pressure and normal contact force change significantly. Among them, the change range of maximum contact pressure is relatively small. The highest decrease in maximum contact pressure when λ = 0 mm can reach 40.55%. In case λ = 1, 2 and 5 mm, the maximum contact pressure decreases by less than 10%. Under different compliance parameters, with the change of contact position in X direction, the normal contact force decreases significantly by about 60%.

In summary, with the movement of the grinding contact position in Y direction, the blade bending deformation intensifies and the contact state changes to a large extent. With the movement of the grinding contact position in X direction, the torsional deformation intensifies and the contact state also changes to varying degrees. For traditional grinding methods with fixed process parameters, the difference in grinding contact state leads to great differences in the material removal effect, ultimately affecting the consistency and integrity of machined surface. Meanwhile, the compliance parameter variation of contact wheel affects the effective contact area between grinding tool and workpiece during machining process, as well as the material removal effect. It can adapt to the changes of characteristics in different blade grinding positions and dynamically control the grinding process.

Using the grinding contact results obtained in the above simulation as the dataset, a total of 180 groups of data were established as shown in Table 3. The compliance parameter λ and different contact positions (x, y) in X and Y directions were used as inputs, and the maximum contact pressure and normal contact force were used as outputs. Among them, 126 groups of sample data were randomly selected as training data sets (accounting for 70%), while 27 groups of data (accounting for 15%) were selected as validation and test data sets, respectively. BP neural network was used to predict the contact characteristic.

Table 3
Input and output data sets

Input			**Output**	
λ/ mm	x/ mm	y/ mm	Maximum pressure/ MPa	Normal contact force/ N
0	0	7.500	0.190	4.611
0	0	12.143	0.188	4.480
0	0	16.786	0.185	4.388
…	…	…	…	…
5	20	72.500	0.055	0.594

Hecht-Nielsen has proved that a 3-layer feedforward network with a hidden layer could approximate any multivariable function [26]. In this manuscript, a prediction model of blade contact characteristic constructed by three-layer BP neural network was used, and the number of nodes in each layer was determined sequentially. As mentioned above, the number of input layer nodes was 3, and the number of output layer nodes was 2. To improve the training efficiency of the network, the hidden layer was set as a single layer, and the initial value of its node number p was selected according to the number of input layer and output layer nodes after comparing the model accuracy and validity.

The structure of the BP neural network-based prediction model for blade grinding contact state was preliminarily determined to be 3-*p*-2. The commonly used training functions include Levenberg-Marquardt (trainlm), Bayesian Regularization (traingbr) and Scaled Conjugate Gradient (trainscg), etc. whose training results are shown in Fig. 15. It can be seen that the trainscg function failed to reach the target accuracy of 1e-04, while the trainbr function achieved the target accuracy 1e-04 after 534 training sessions. As for the trainlm function, it reached 5.646e-05 only after 82 training sessions, which met the accuracy requirements and had a fast convergence speed. Hence, the trainlm was selected as the training function for the BP neural network-based prediction model.

By setting the hidden layer node number of the trainlm-based BP neural network separately at 5, 7, 9 and 10, the root-mean-square error was obtained by calculating the network model several times, and the results are detailed in Table 4. The node number of the network hidden layer was determined to be 10.

Table 4
Mean square error of prediction model under different number of hidden layer nodes conditions

hidden layer nodes	**5**	**7**	**9**	**10**
Mean square error	2E-3	2.5E-3	3E-4	5.6E-5

The topological structure of the constructed BP neural network was 3-10-2, and its learning rate was lr = 0.01. The maximum training epochs were set as 1,000, while the allowable error was set as 0.001. The BP neural network model was constructed in MATLAB, and sample data were used to train the network. The contact characteristic prediction model was established finally. As shown in Fig. 16 (a), the training regression R is very close to 1. And as shown in Fig. 16 (b), the network training error is less than 0.001 at 82 steps, which achieving the training goal.

The Generalization ability of neural network refers to the ability of BP neural network to predict uncertain data. Despite a powerful generalization function of BP neural network for information within the range of training samples, whether it can attain higher estimation accuracy for information outside the training sample range is the core of evaluating the training model [27]. Therefore, the generalization ability of the above-mentioned neural network model was tested, and 6 groups of original data sets that do not exist in the training sample were added for verification of the neural network prediction model as shown in Table 5.

Table 5
Comparison between simulation and prediction results

Sample data	Conditions			Simulation results		Prediction results	
	λ/ mm	*x*/ mm	*y*/ mm	Maximum pressure/ MPa	Normal contact force/ N	Maximum pressure / MPa	Normal contact force/ N
1	3	5	13	0.0993	3.04	0.1095	3.24
2	3	5	39	0.0809	2.18	0.0888	2.32
3	3	5	65	0.0621	1.35	0.0712	1.56
4	1.5	15	13	0.0944	2.74	0.1062	2.40
5	1.5	15	39	0.0730	1.77	0.0788	1.52
6	1.5	15	65	0.0526	0.96	0.0567	0.82

The neural network predictions were comparatively analyzed and compared with the finite element simulation results as shown in Fig. 17. Taking the simulation data as the true value, the relative error of predicted maximum contact pressure is 14.65% at highest and 7.80% at lowest, while the relative error of predicted normal contact force is 15.56% at highest and 6.48% at lowest. The relative errors are all small, proving high reliability of the neural network-based prediction model, which can accurately predict the grinding contact state of blade at different machining positions. The findings provide guidance for regulating the blade surface precision and quality consistency, and improving the uncertain effect of blade rigidity difference on machining quality.

7. Conclusions

1. In response to the problems of easy deformation and poor consistency of machining thin-walled aircraft blades, a novel abrasive belt grinding technique with adjustable compliance is proposed based on the blade structure characteristics and fixture characteristics. The simulation results verify that the proposed adjustment method has a significant impact on the processing state. Under different compliance parameters, the normal contact force changes significantly, with a maximum change rate of 30.80%, which can affect the blade grinding contact state and contribute to obtain consistent processing quality.

2. Contact state variations in different grinding positions along the directions of blade width and length are separately explored. With the change of grinding position in the direction of blade width, the wall thickness of the blade decreases, and the rigidity weakens. The contact pressure distribution gradually becomes uniform, and the normal contact force decreases rapidly, with a maximum decrease rate of 65.43%. With the change of the grinding position in the direction of blade length, the support rigidity of

blade weakens, and the contact pressure distribution becomes more uniform to present an overall elliptical distribution. The normal contact force decreases significantly, with a maximum decrease rate of 68.49%. Compared with experimental results, it is found that both average absolute percentage error and root mean square error are small, indicating that simulation results have high reliability.

3. Considering multiple factors such as compliance parameter and different contact positions in blade width and length directions during grinding contact process, grinding contact state data are obtained. Based on BP neural network, a prediction model for maximum contact pressure and normal contact force is established. The average absolute percentage errors of prediction model are 10.50% and 11.67%, respectively. The relative errors are relatively small, which verifies that prediction model has high reliability. The developed model can accurately predict the contact characteristics at different grinding positions, which provides guidance for improving the stability of blade grinding quality.

Declarations

Funding

This work was supported by the Natural Science Basic Research Program of Shaanxi (Grant numbers 2023-JC-YB-434 and 2022JM-240) and the Key Research and Development Program of Shaanxi (Grant numbers 2021ZDLGY09-01).

Competing interests

The authors have no relevant financial or non-financial interests to disclose.

Author contribution

All authors contributed to the study conception and design. Material preparation, data collection and analysis were performed by Jihao Duan, Zhuofan Wu and Jiale An. Dou Wang, Feng Gao and Wenbo Huai participated in carrying out grinding experiments. The first draft of the manuscript was written by Jihao Duan and all authors commented on previous versions of the manuscript. All authors read and approved the final manuscript.

Acknowledgements

This work was supported in part by the Natural Science Basic Research Program of Shaanxi under Grant 2023-JC-YB-434 and 2022JM-240, in part by Key Research and Development Program of Shaanxi under Grant 2021ZDLGY09-01.

References

1. Huang Y, Xiao GJ, Zou L (2019) Current situation and development trend of robot precise belt grinding for aero-engine blade [J]. Acta Aeronautica et Astronautica Sinica 40(3):48–67

2. Zhu D, Xu X, Jiang C et al (2021) Research progress in robotic grinding technology for complex blades [J]. Acta Aeronautica et Astronautica Sinica 42(10):8–30
3. Huang Y, Hou M, Liu Y et al (2020) Robotic floating belt grinding technology and experimental study on aero-engine titanium alloy blade [J]. Aeronaut Manuf Technol 63(5):14–19
4. Chen G, Yang J, Yao K et al (2023) Robotic abrasive belt grinding with consistent quality under normal force variations [J]. Int J Adv Manuf Technol 125(7–8):3539–3549
5. Jia H, Lu X, Cai D et al (2023) Predictive Modeling and Analysis of Material Removal Characteristics for Robotic Belt Grinding of Complex Blade [J]. Appl Sci 13(7):4248
6. Fan WG, Wang WX, Hou GY et al (2020) Macro Contact Pressure Modeling and Simulation for Rail Grinding with Abrasive Belt Based on Curvature Match [J]. J Mech Eng 56(02):154–162
7. Xu X, Chen W, Zhu D et al (2021) Hybrid active/passive force control strategy for grinding marks suppression and profile accuracy enhancement in robotic belt grinding of turbine blade [J], vol 67. Robotics and Computer-Integrated Manufacturing, p 102047
8. Zhang H, Li L, Zhao J et al (2021) The hybrid force/position anti-disturbance control strategy for robot abrasive belt grinding of aviation blade base on fuzzy PID control [J]. Int J Adv Manuf Technol 114(11–12):3645–3656
9. Wang Q, Wang W, Zheng L et al (2021) Force control-based vibration suppression in robotic grinding of large thin-wall shells [J], vol 67. Robotics and Computer-Integrated Manufacturing, p 102031
10. Zhang T, Xiao M, Zou Y et al (2020) Robotic constant-force grinding control with a press-and-release model and model-based reinforcement learning [J]. Int J Adv Manuf Technol 106:589–602
11. Wang Z, Zou L, Luo G et al (2022) A novel selected force controlling method for improving robotic grinding accuracy of complex curved blade [J]. ISA Trans 129:642–658
12. Kara F, Köklü U, Kabasakaloğlu U (2020) Taguchi optimization of surface roughness in grinding of cryogenically treated AISI 5140 steel[J]. Mater Test 62(10):1041–1047
13. Li F, Xue Y, Zhang Z et al (2020) Optimization of grinding parameters for the workpiece surface and material removal rate in the belt grinding process for polishing and deburring of 45 steel [J]. Appl Sci 10(18):6314
14. Awale AS, Vashista M, Yusufzai MZK (2020) Multi-objective optimization of MQL mist parameters for eco-friendly grinding [J]. J Manuf Process 56:75–86
15. Zhang T, Yu Y, Yang L et al (2020) Robot grinding system trajectory compensation based on co-kriging method and constant-force control based on adaptive iterative algorithm [J]. Int J Precis Eng Manuf 21:1637–1651
16. Xu Q, Li X, Huo X (2022) A Neural Network Error Compensation Technology for Precision Grinding Based on Genetic Algorithm[C]. 2022 International Conference on Artificial Intelligence and Autonomous Robot Systems (AIARS). IEEE, : 319–323
17. Yuan LJ (2021) The Method and Experimental Research on Improving Quality and Effciency of Aeroengine Blade Belt Grinding [D]. Chongqing University

18. Xu XH, Zhu DH, Zhang H et al (2019) Application of novel force control strategies to enhance robotic abrasive belt grinding quality of aero-engine blades [J]. Chin J Aeronaut 32(10):2368–2382
19. Xu X, Chen W, Zhu D et al (2021) Hybrid active/passive force control strategy for grinding marks suppression and profile accuracy enhancement in robotic belt grinding of turbine blade[J]. Robot Comput Integr Manuf 67:102047
20. Zhang T, Xiao M, Zou Y et al (2020) Robotic constant-force grinding control with a press-and-release model and model-based reinforcement learning [J]. Int J Adv Manuf Technol 106(1):589–602
21. Khalick Mohammad AE, Hong J, Wang D (2017) Polishing of uneven surfaces using industrial robots based on neural network and genetic algorithm [J]. Int J Adv Manuf Technol 93(1):1463–1471
22. Chen F, Zhao H, Li D et al (2019) Contact force control and vibration suppression in robotic polishing with a smart end effector [J]. Robot Comput Integr Manuf 57:391–403
23. Zhou ZW (2022) Research on Contact Characteristics of Belt Grinding of Aero-engine Blade based on Compliance Adjustment of Contact Wheel [D].
24. Duan JH, Zhou ZW, An JL et al (2023) Research on Contact Characteristics of Belt Grinding of Aero-engine Blade Based on Compliance Adjustment of Contact Wheel [J]. Journal of Mechanical Engineering, http://kns.cnki.net/kcms/detail/11.2187.TH.20230428.1445.032.html. (on line)
25. Chen JZ, Huang MX, Wang XR et al (2015) Typical Constitutive Models of Rubber Materials and Their Ranges of Application [J]. Mater Rep 29(S1):118–120
26. Hecht-Nielsen R (1989) Theory of the backpropagation neural network [M]. Neural networks for perception. Harcourt Brace & Co 2:593–605

Figures

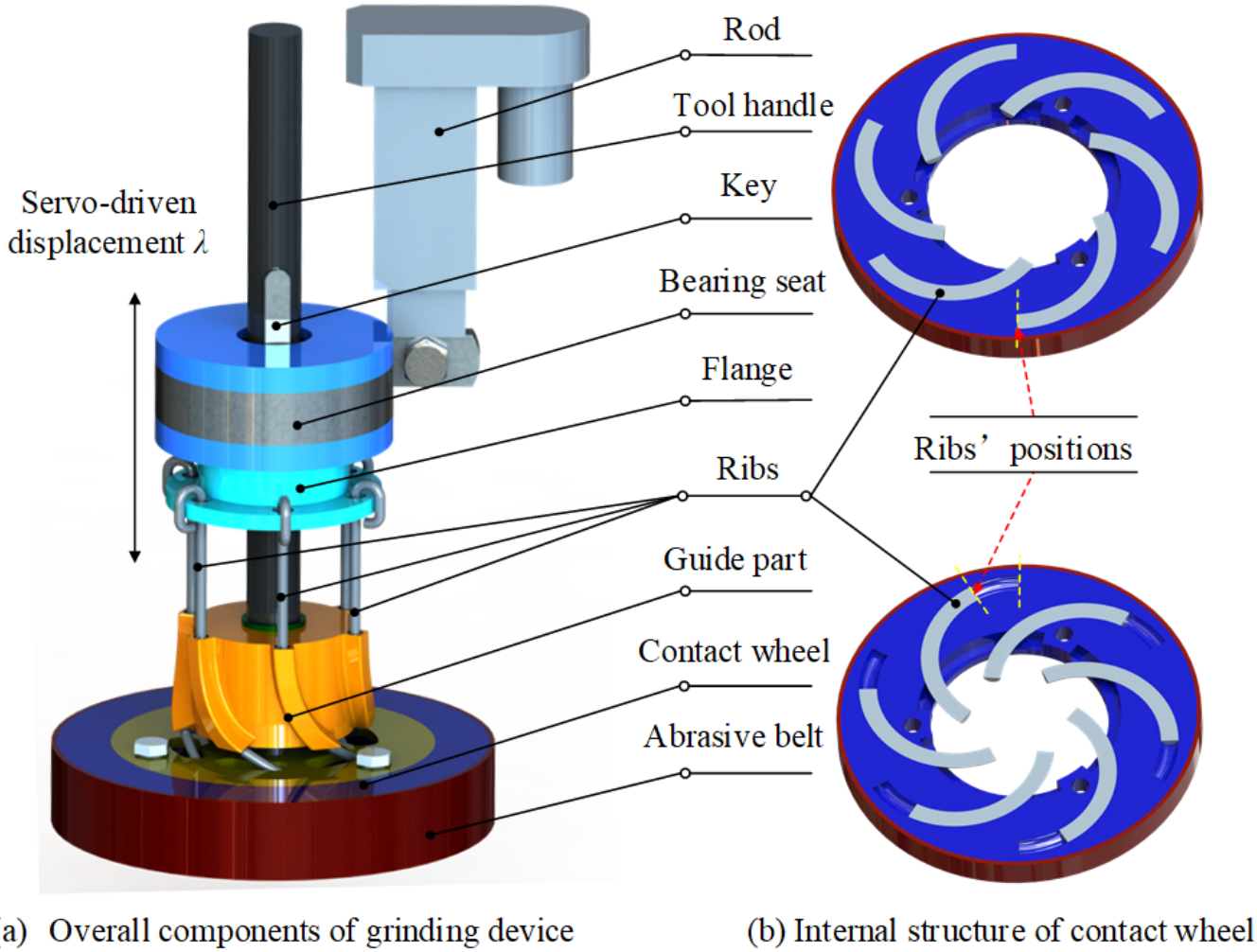

Figure 1

grinding device with compliance adjustable contact wheel

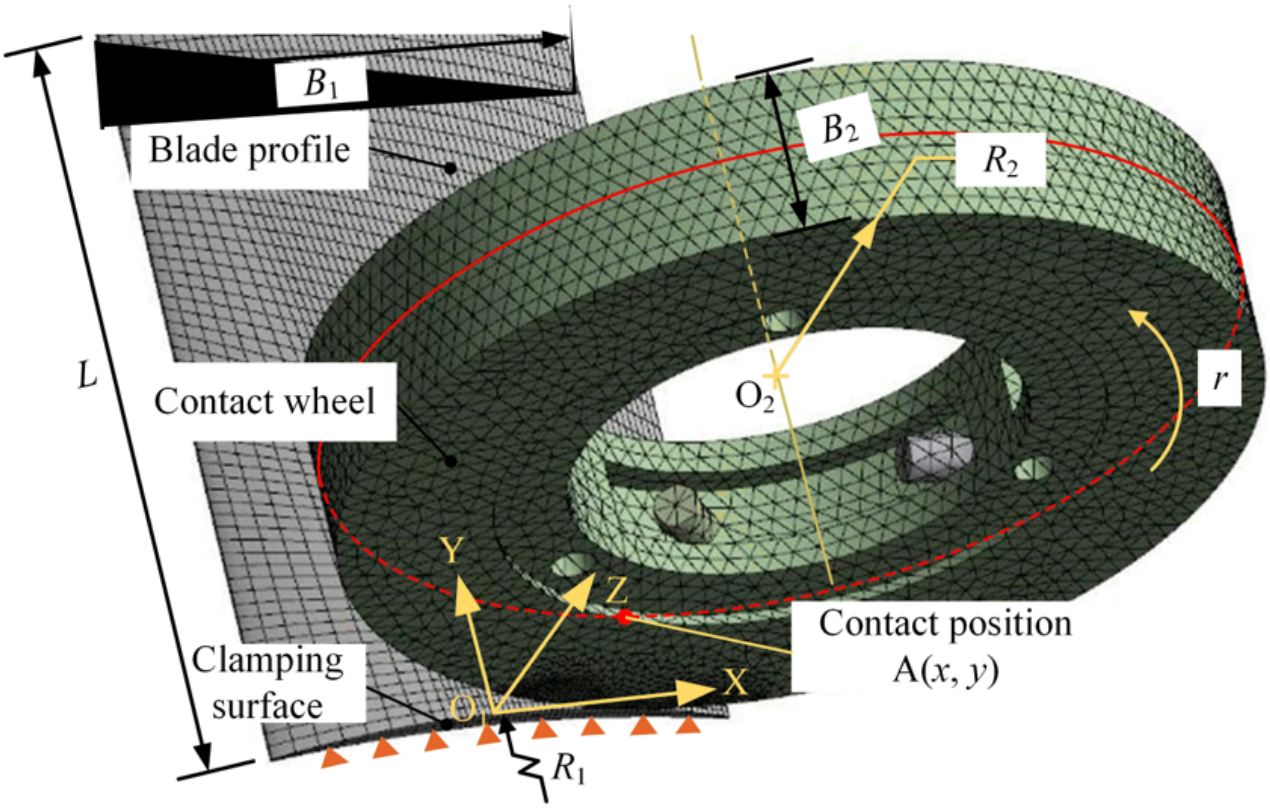

Figure 2

Contact model of wheel and blade

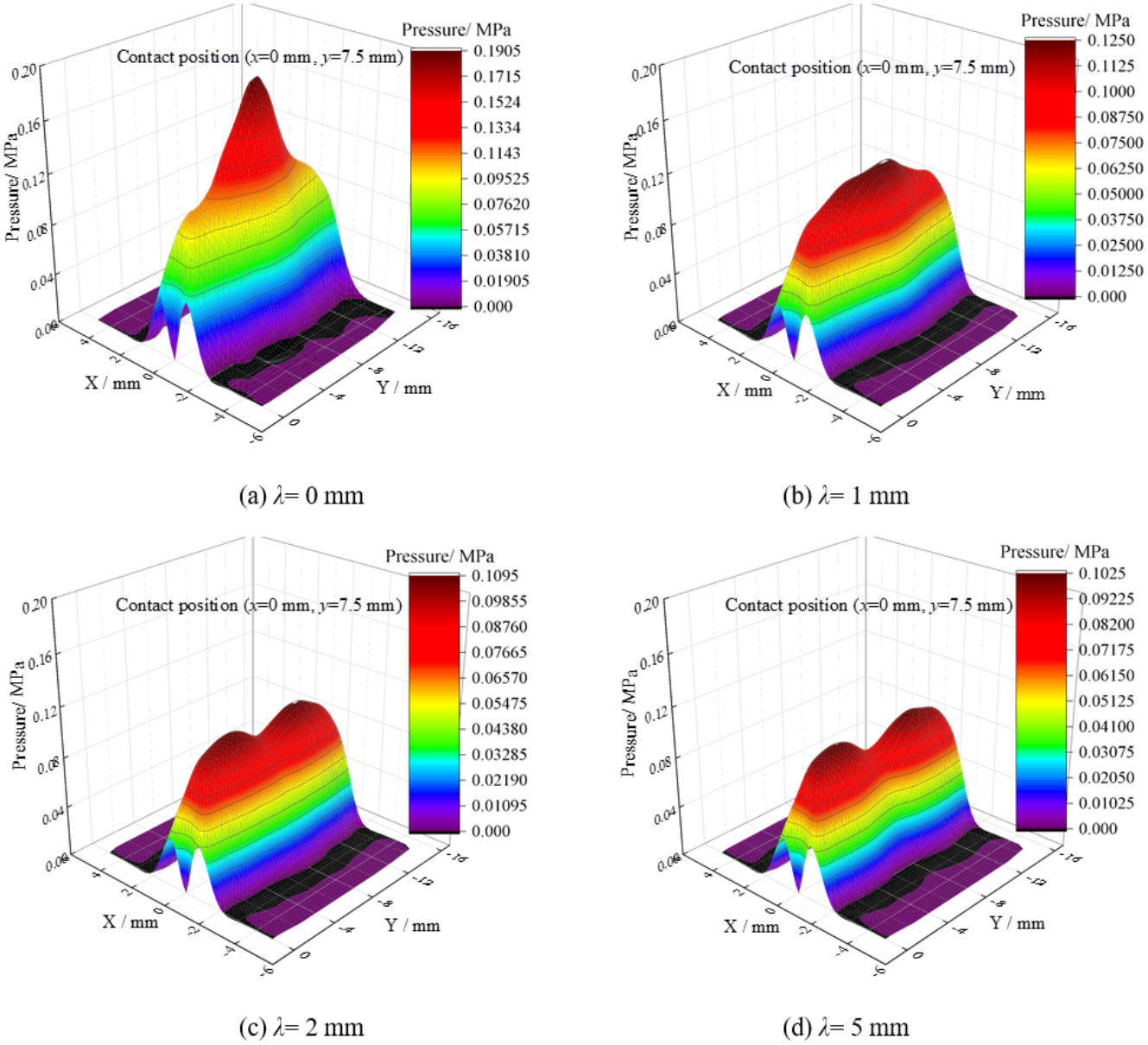

Figure 3

Effect of different wheel compliance λ on the distributions of grinding contact pressure

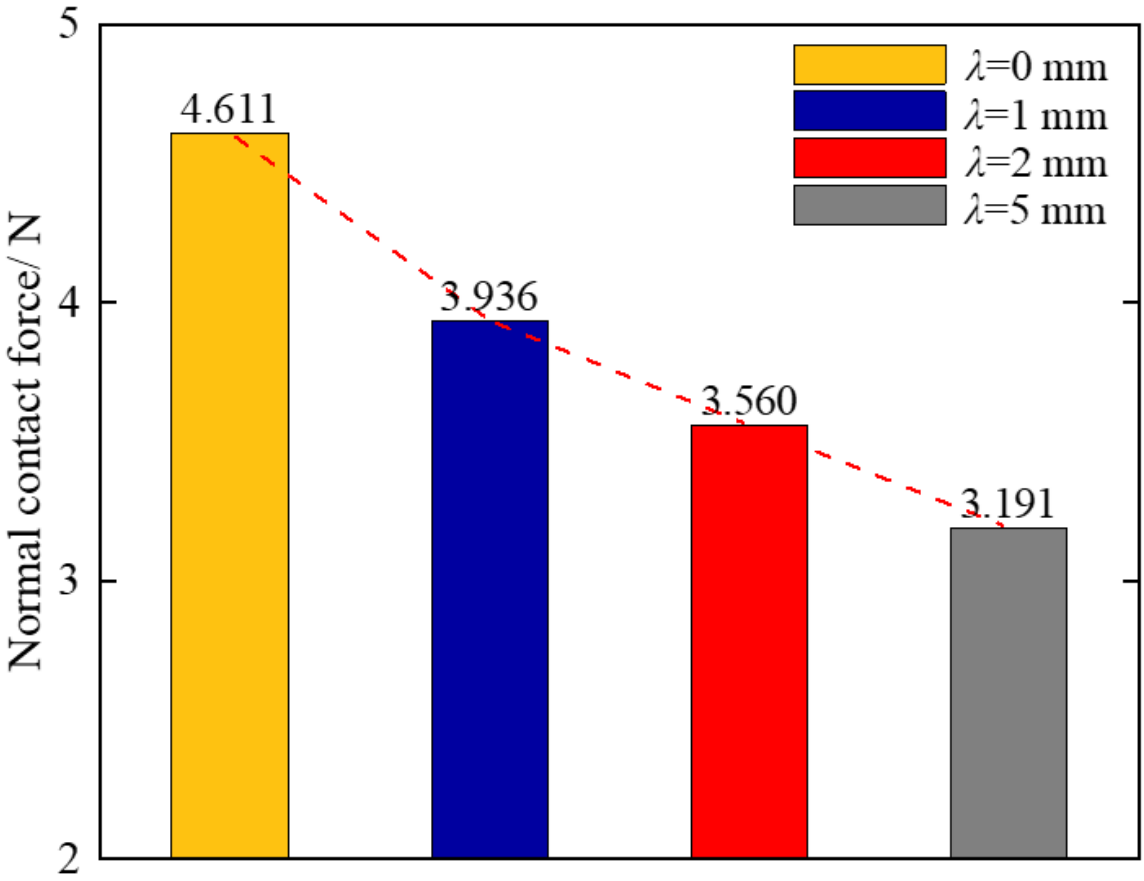

Figure 4

Effect of λ on equivalent normal contact force

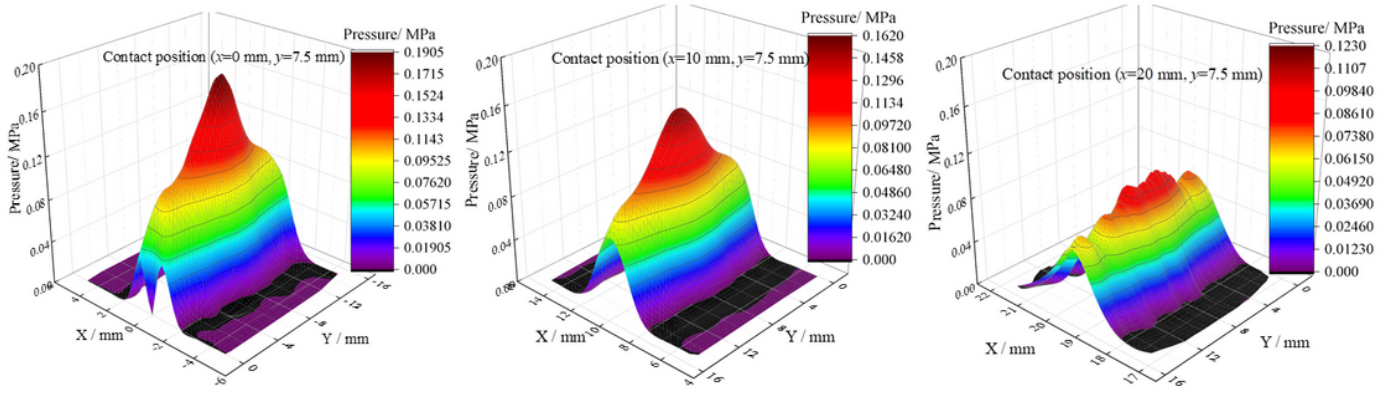

(a) x=0 mm (b) x=10 mm (c) x=20 mm

Figure 5

Pressure distribution at different positions in X direction when λ= 0 mm

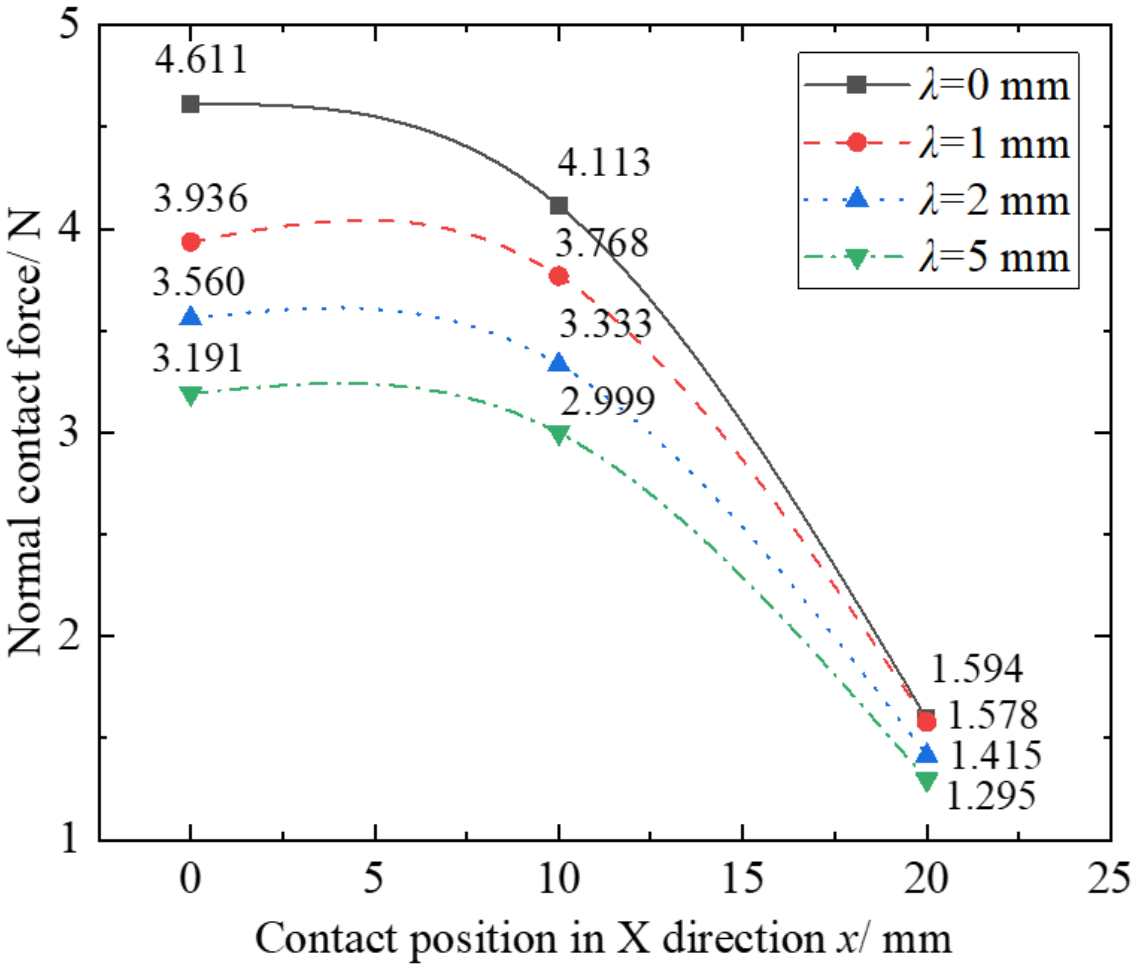

Figure 6

Equivalent normal contact force at different positions in X direction

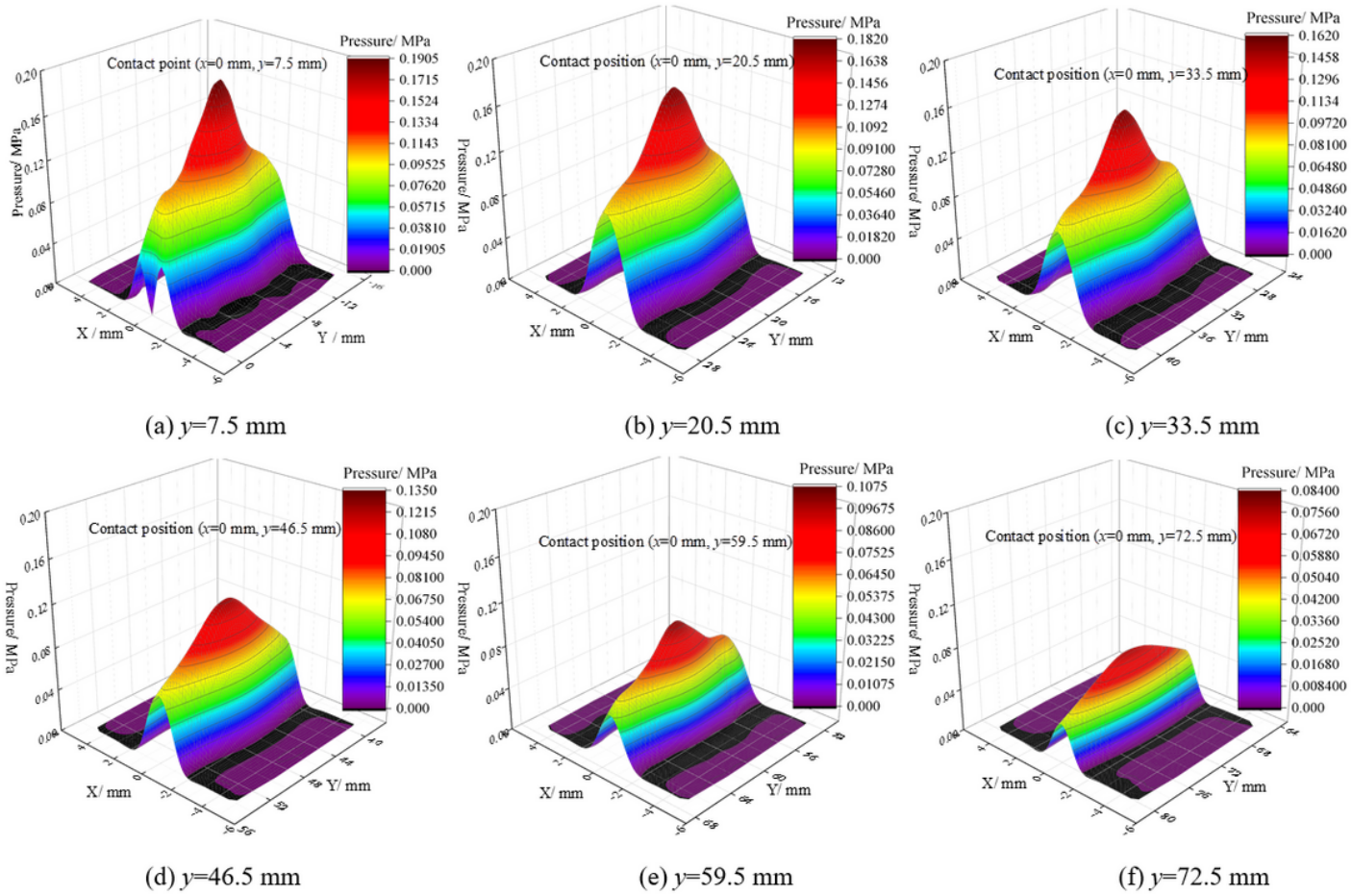

Figure 7

Pressure distribution at different positions in Y direction when λ = 0 mm

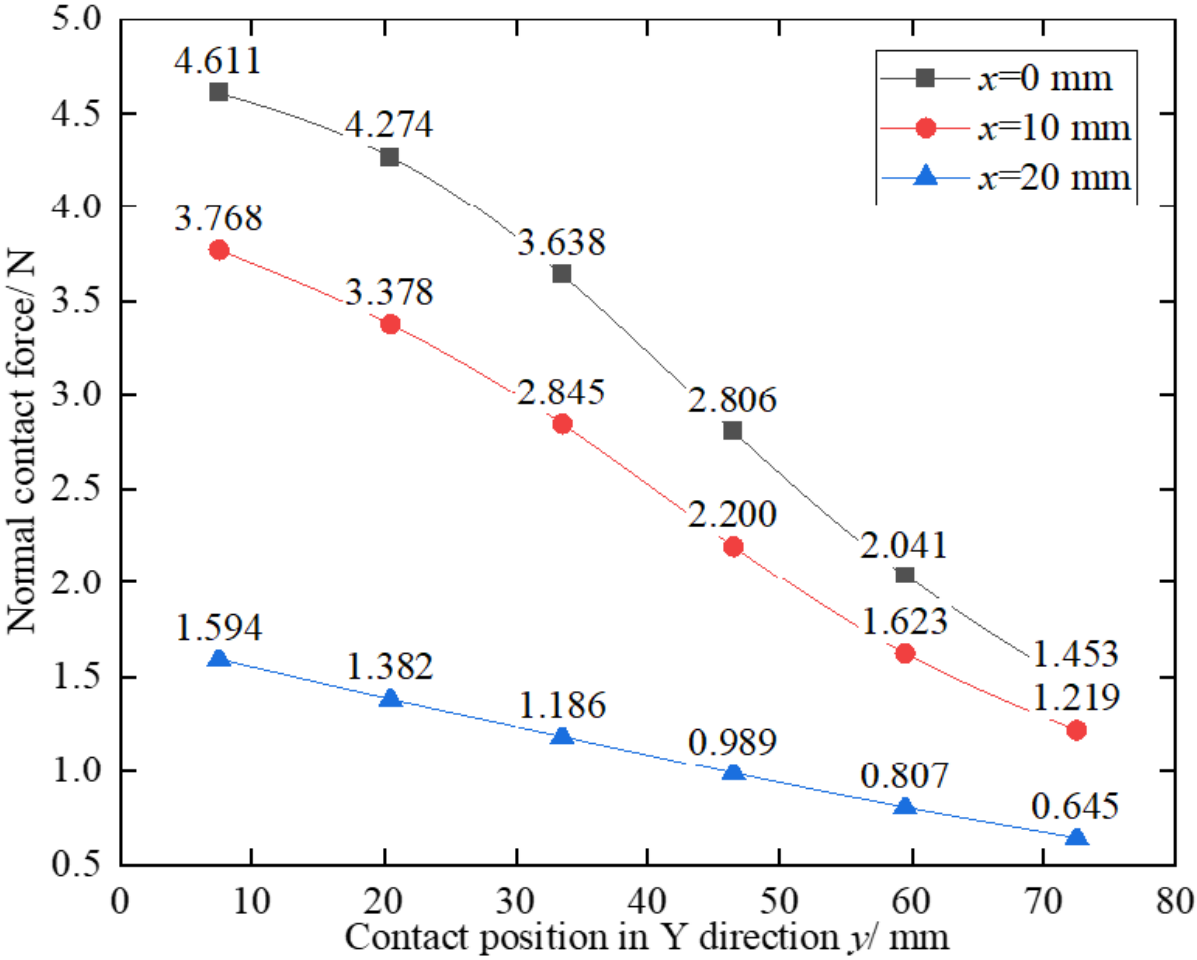

Figure 8

Equivalent normal contact force at different positions in Y direction

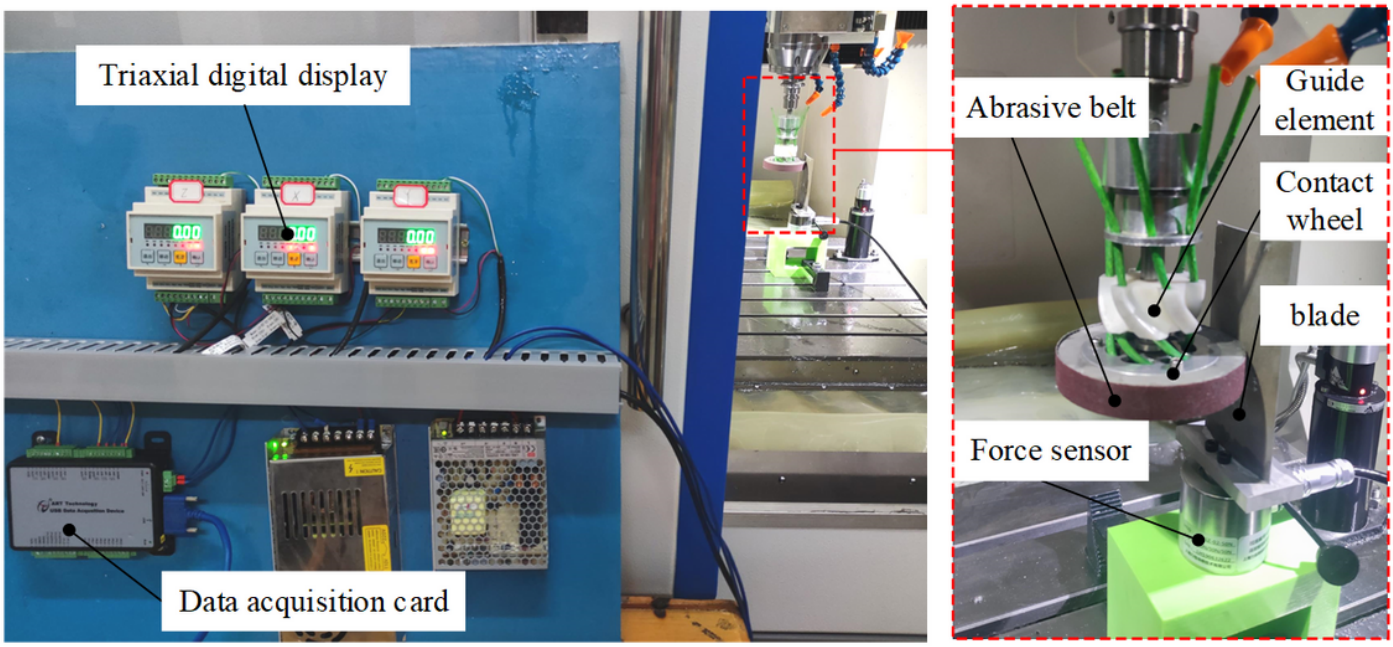

Figure 9

The grinding experimental setup

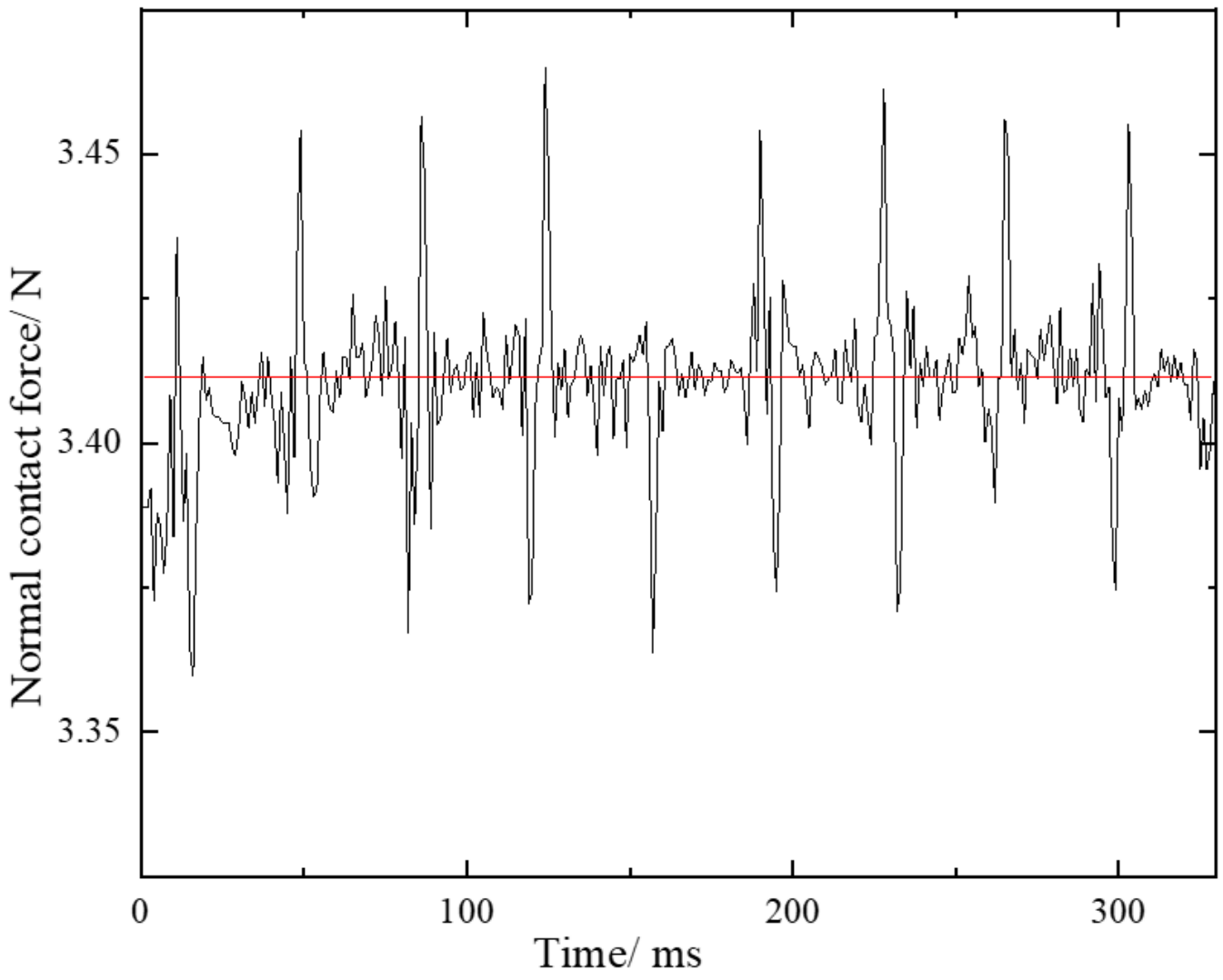

Figure 10

Normal grinding force data acquisition

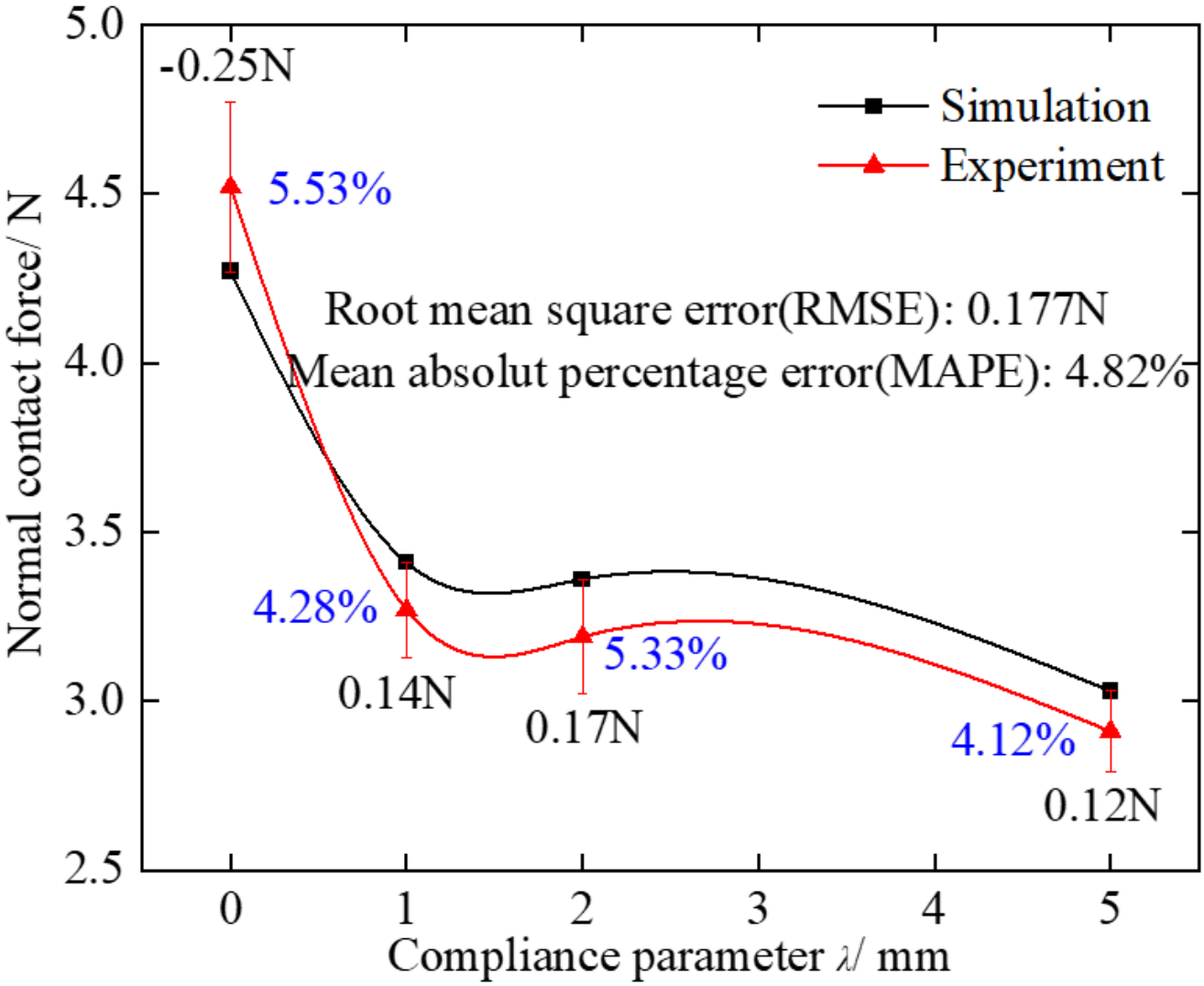

Figure 11

Experimental results with different compliance parameters

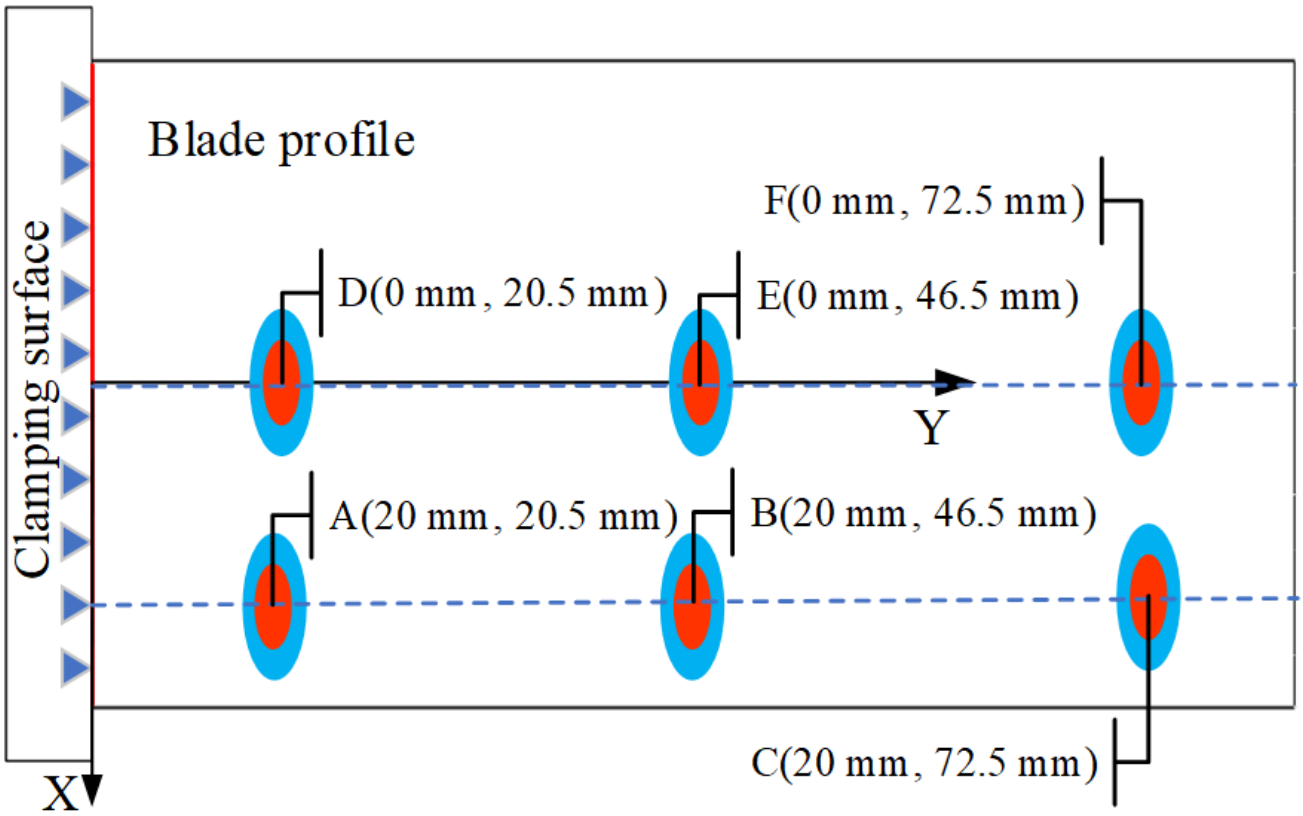

Figure 12

Grinding positions of the blade

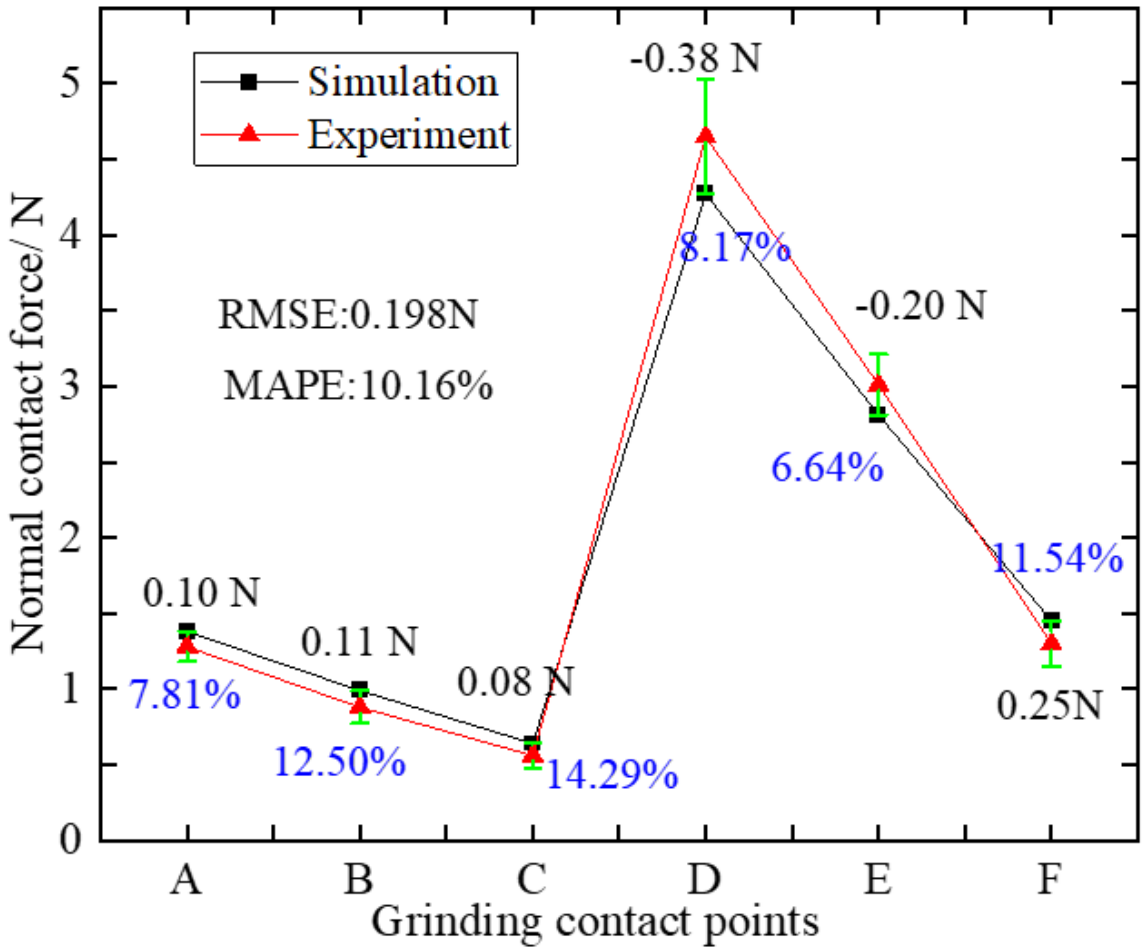

Figure 13

Normal contact force at different positions of the blade

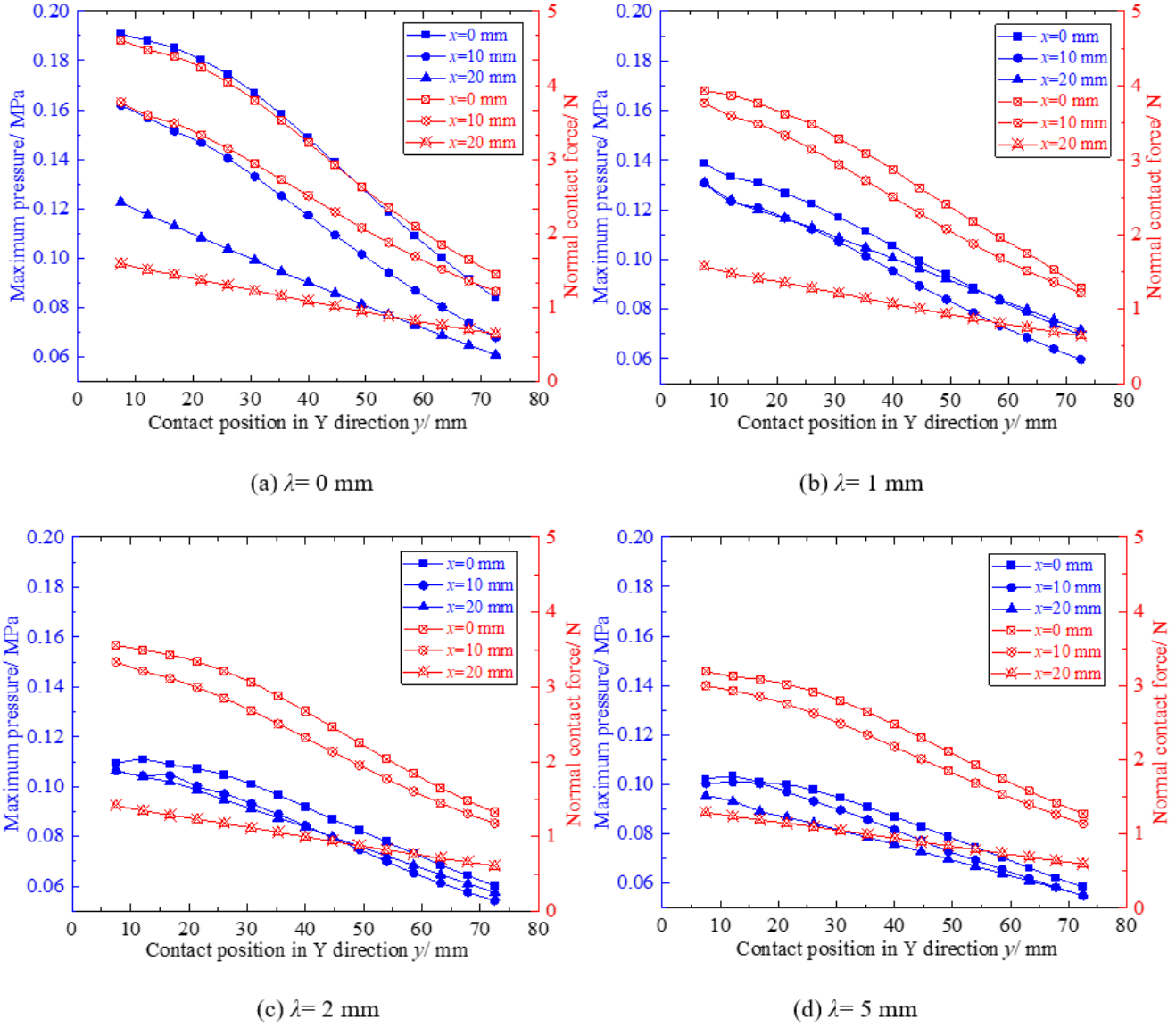

Figure 14

Variation of maximum pressure and normal force under different conditions

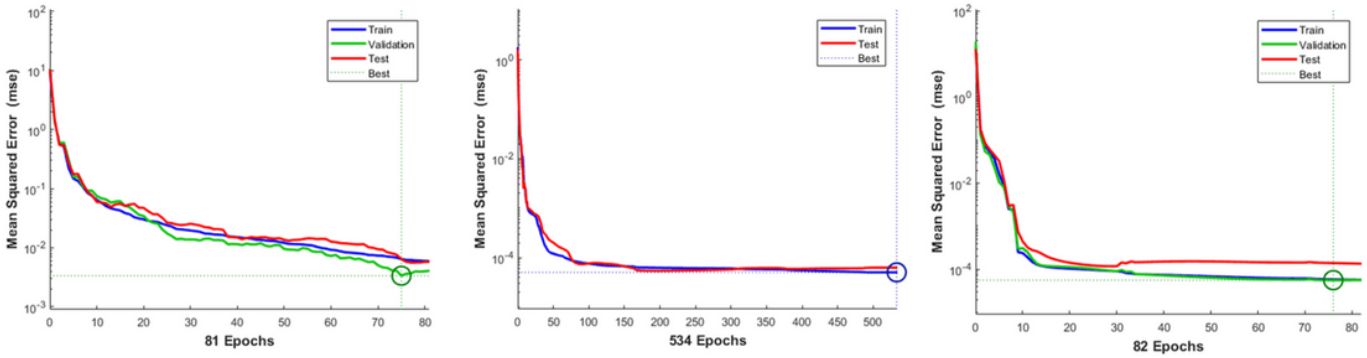

Figure 15

Comparison of training accuracy of different training functions

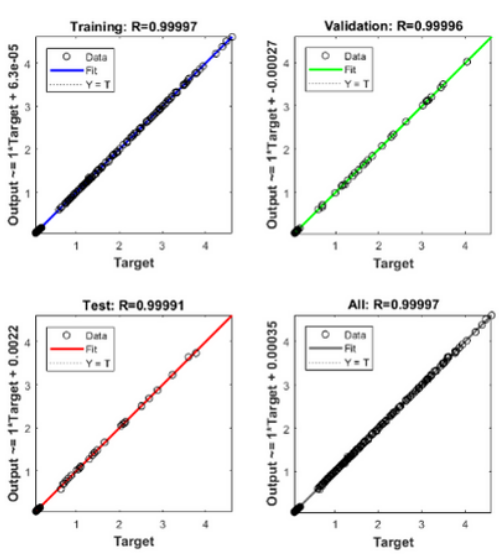

(a) Training regression analysis

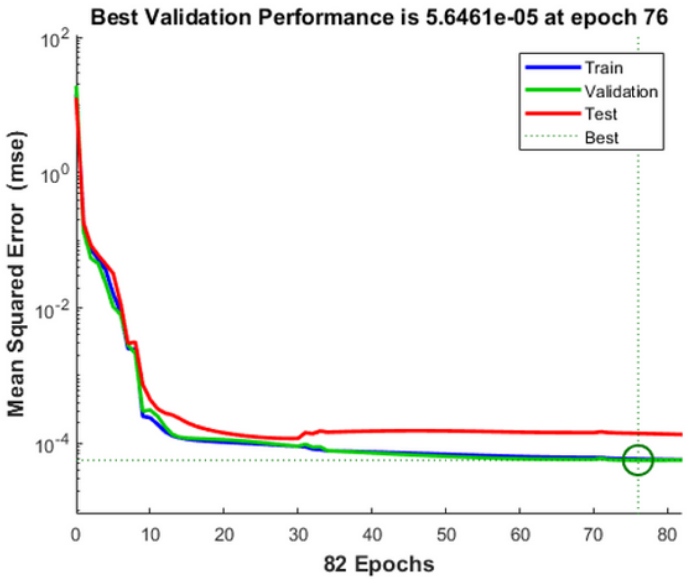

(b) Mean squared error of training model

Figure 16

Training results of BP Neural Network

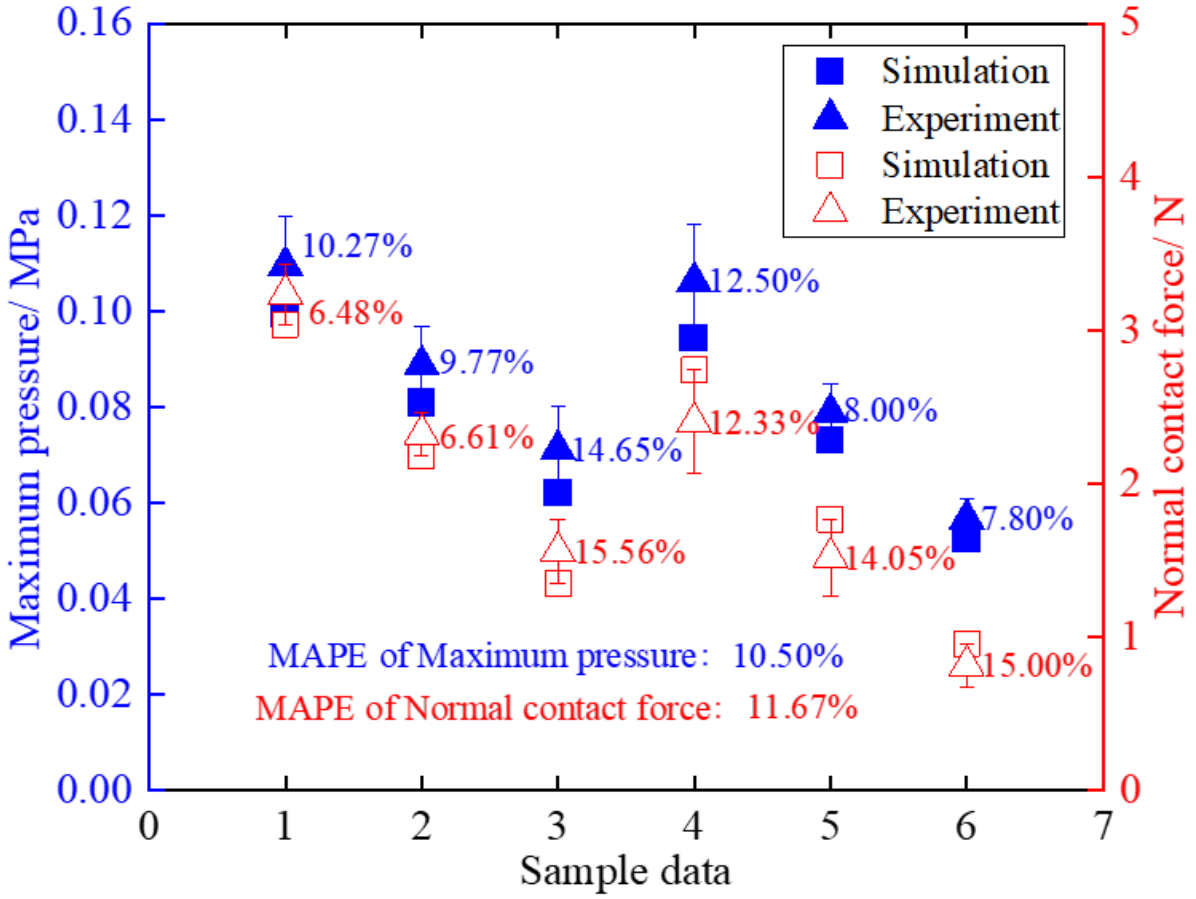

Figure 17

Comparison between simulation and prediction results